View metadata, citation and similar papers at core.ac.uk
brought to you by CORE
provided by Griffith Research Online

Transition between amorphous and crystalline phases of SiC deposited on Si substrate using H_3SiCH_3

Li Wang,[1,*] Sima Dimitrijev, [1] Jisheng Han, [1] Francesca Iacopi[1,2] and Jin Zou [3]

[1]*Queensland Microtechnology Facility and Griffith School of Engineering, Griffith University, Nathan, Qld. 4111, Australia,*

[2]*Interuniversity Microelectronics Centre, Kapeldreef 75, 3001 Leuven, Belgium,*

[3]*Centre for Microscopy and Microanalysis and School of Engineering, The University of Queensland, St. Lucia, Qld. 4072, Australia*

This paper presents a study of the transition between amorphous and crystalline phases of SiC films deposited on Si(100) substrate using H_3SiCH_3 as a single precursor by a conventional low-pressure chemical vapor deposition method in a hot-wall reactor. The microstructure of SiC, characterized by x-ray diffraction and high-resolution transmission electron microscopy, is found to vary with substrate temperature and H_3SiCH_3 pressure. The grain size decreases with increasing MS pressure at a given temperature and also decreases with reducing temperature at a given MS pressure. The deposition rates are exponentially dependent on the substrate temperature with the activation energy of around 2.6 eV. The hydrogen compositional concentration in the deposited SiC films, determined by secondary ion mass spectrometry depth profiling, is only 2.9 % in the nanocrystalline SiC but more than 10 % in the amorphous SiC, decreasing greatly with increasing deposition temperature. No hydride bonds are detected by Fourier transform infrared spectroscopy measurements. The chemical order of the deposited SiC films improves with increasing deposition temperature.

Keywords: A1. Crystal structure, A1. X-ray diffraction, A3. Chemical vapor deposition processes, B1. Nanomaterials, B1. Amorphous, B1. Silicon Carbide.

PACS codes: 68.37.Og, 68.55.ag, 81.05.Gc, 81.07.Bc, 81.15.Gh, 82.80.Ej.

*Corresponding author: Li Wang

Postal address:
Queensland Microtechnology Facility
Griffith University, Nathan QLD 4111
Australia

Telephone: +61-7-37358006

Fax: +61-7-37358021

Electronic mail: l.wang@griffith.edu.au

1. Introduction

Amorphous Si_xC_{1-x} (a-SiC) and nanocrystalline silicon-carbide (nc-SiC) have attracted a considerable research interest as materials for constructing high-efficiency silicon solar cells [1-5]. Amorphous SiC is also applied as a passivation layer for crystalline silicon [6] and as a metal diffusion barrier for copper [7]. Various growth techniques have been employed to achieve gaseous reactive species when the substrate temperature is relatively low, including bias-assisted hot filament chemical vapor deposition [8], plasma-enhanced chemical vapor deposition (PECVD) [9, 10], pulsed laser deposition [11], and ion beam sputtering [12]. Compared with these techniques, the conventional chemical vapor deposition (CVD) requires higher deposition temperatures. However, higher temperatures may enhance the chemical order [13, 14], therefore can increase the optical energy gap of the grown materials and improving their doping efficiency [15-17]. It has been reported [18] that the highest structural order in amorphous films is achieved just before the transition from amorphous to crystalline phase.

The preparation of a-SiC is usually conducted with two precursors that are heavily diluted by hydrogen to hydrogenate the dangling bonds and to widen the optical energy gap by reducing the homonuclear Si–Si, and C=C graphic bonds. The density, thermal stability, optical and photoelectrical properties are strongly correlated to the bonding configuration and H concentration in these a-SiC films. Si–H and C–H bonds start to release H at 327 and 577ºC, respectively, which causes thermal instability, and all the H atoms escape from the film at temperature higher than 800 ºC [19]. Therefore, the thermal stability of the films can be improved with the higher deposition temperature.

As a promising single precursor for single-crystalline SiC deposition, H_3SiCH_3 (methylsilane, abbreviated as MS) has recently been widely investigated in various deposition

methods [20-25]. Because Si–C bonds are already present in MS with the Si:C ratio of 1:1, MS is a desirable precursor for the preparation of chemically ordered a-SiC films in the region close to the amorphous-to-crystalline transition. Deposition of a-SiC films using MS has been achieved by different techniques, including electron beam excitation [26], hot-wire CVD [27], PECVD [28], and cold-wall CVD [29]. Although it is understood that the amorphous-to-crystalline transition temperature depends on the preparation method and processing pressure, there is no study on the transition from a-SiC to crystalline SiC (c-SiC) for films deposited by the conventional low-pressure CVD (LPCVD) method in a hot-wall reactor with MS as a single precursor. Such a study can provide the guidance for the development of deposition phase diagrams and is of significant technological importance for the preparation of chemically ordered a-SiC or partly crystallized nc-SiC films.

In this study, we investigate a-SiC and c-SiC films deposited on Si substrates, in the temperature range between 600 and 700 ºC, using MS as a single precursor in a conventional hot-wall LPCVD reactor. The microstructures and chemical order of the deposited SiC films were investigated by various characterization techniques. The analysis is focused on the factors controlling the structural transition, H concentration and bonding configuration in the deposited SiC films.

2. Experimental details

SiC films were deposited on Si(100) substrates (a resistivity of 5-15 Ω·cm) using MS as the precursor in a hot wall LPCVD reactor (with a base pressure lower than 5×10^{-8} mbar). The deposition of SiC films was carried out in the temperature range of 600-700 ºC (in the 50 ºC interval) with the MS pressure ranging from 0.006 to 0.06 mbar. The flow rate of MS was maintained at 9.5 sccm for all deposition processes, and the duration of each deposition process was set to be 10 h. Prior to the loading of Si substrates into the LPCVD reactor,

standard RCA clean was carried out. The temperature was ramped to the desired deposition temperature in vacuum with a ramp speed of 5 ºC /min.

X-ray diffraction (XRD) analysis, high-resolution transmission electron microscopy (HRTEM), secondary ion mass spectrometry (SIMS) and Fourier transform infrared (FTIR) spectroscopy were employed to characterize the deposited SiC films. The XRD measurements were performed with CuKα radiation in a Bruker D8 advance x-ray diffractometer, with acquisitions from 20º to 75º, an increment of 0.02 º/step, and the duration for each step of 2.4 seconds. The HRTEM measurements were carried out on cross-section TEM specimens using a FEI Tecnai F30 TEM (operating at 300 kV). The SIMS measurements for H depth profiling analysis were carried out using a Cameca IMS-5f ion microprobe equipped with a double focusing magnetic sector using Cs^+ source. The detection limit of H in Si is 2×10^{20} cm^{-3} and the precision of SIMS depth analysis for SiC material is ±15 %. The FTIR absorption spectrum measurements were performed by a NexusTM spectrometer from Nicolet in the mid-IR range from 400 to 4000 cm^{-1} with a resolution of 4 cm^{-1}. The reference spectrum of a fresh Si wafer was subtracted.

Detailed growth conditions and SiC film thickness for different samples are summarized in Table. 1, where the deposition rates can be determined by dividing the deposited film thickness by 10 h. The sample labels are given in the forms of Txxx_LP and Txxx_HP, in which the number xxx represents the process temperature (in ^oC), LP stands for “low pressure” and is used for samples processed at 0.006mbar, and HP stands for “high pressure” and is used for samples processed at 0.06mbar.

Table 1. Detailed growth conditions and SiC film thickness for different samples.

3. Results and discussion

3.1 The microstructure of deposited SiC films

3.1.1 Influence of substrate temperature on the microstructure of deposited films

The dependences of the deposition rates on the substrate temperature are shown in Fig. 1. The deposition rates are exponentially dependent on the substrate temperature with the activation energy of about 2.6 eV for both pressures. For sample T600_LP, the deposition rate

Fig. 1. The dependences of deposition rates on the substrate temperature and MS pressure.

is too slow to yield a desirable thickness for further characterizations. XRD patterns for all 5 samples (except T600_LP) are shown in Fig. 2. Figure 3 shows the cross-section HRTEM images and corresponding selected area electron diffraction (SAED) patterns for samples T700_LP, T700_HP, T650_HP and T600_HP. A relative sharp diffraction peak at 2θ around 35.8º is found (as shown in Fig. 2) for sample T700_LP, corresponding to 3C-SiC{111} diffractions. Crystal lattice fringes are observed in sample T700_LP (shown in Fig. 3(a)), and four homocentric diffraction rings are seen in Fig. 3(b), identified as 3C-SiC (111), (200), (220) and (311) reflections, respectively. The regular dot diffractions are from underlying Si in SAED patterns in Fig. 3(b) and (h). Lower magnification TEM images (not shown here) show that crystal grains have a columnar shape that expands laterally up to 100 nm as the film thickness is increasing. All these results indicate that sample T700_LP is composed of nc-SiC. For sample T650_LP, a much broader diffraction peak is found in XRD patterns (as shown in Fig. 2), indicating grain size becomes smaller when deposition temperature was reduced from 700 to 650 ^{o}C. No pure a-SiC was observed with MS pressure of 0.006mbar.

Fig. 2. X-ray diffraction patterns for SiC films deposited under various conditions.

Fig. 3. (a) HRTEM image of sample T700_LP, (b) SAED patterns of sample T700_LP, the regular dot diffractions are from underlying Si substrate (c) HRTEM image of sample T700_HP, (d) SAED patterns of sample T700_HP, (e) HRTEM image of sample T650_HP, (f) SAED patterns of sample

T650_HP, (g) HRTEM image of sample T600_HP, (h) SAED patterns of sample T600_HP, the regular dot diffractions are from underlying Si substrate.

For samples deposited with MS pressure of 0.06mbar, there is a broad diffraction peak at 2θ around 35.8º in the XRD patterns from sample T700_HP. Crystal lattice fringes are observed in Fig. 3(c), the grain size is in the range of 5 to 10 nm, and three circular rings are found in the SAED patterns in Fig. 3(d), identified as reflections from 3C-SiC (111), (220) and (311), respectively. No diffraction peaks in the XRD patterns can be found for samples T650_HP and T600_HP, which reveals that they are pure amorphous in structure. No crystal fringes can be found in the HRTEM images as shown in Fig. 3(e) and (g). The diffused rings in Fig. 3(f) and (h) confirm that these films are amorphous in structure. The experimental results from XRD and TEM are in good agreement; both demonstrate that the nucleation of crystal grains are inhibited at reduced deposition temperature, and pure a-SiC was deposited onto Si substrate when the temperature is equal or below 650ºC with a MS pressure of 0.06 mbar.

3.1.2 The effect of pressure on the microstructure of deposited films

The effect of pressure on the microstructure of deposited films can be determined by the comparison of films deposited under different pressures. The dependences of the deposition rates on MS pressure are also shown in Fig. 1. For samples T700_LP and T700_HP, an increasing of 10 times in MS pressure leads to a 2.6 times increase in the deposition rate, from 41 to 105 nm/h. The same trend is also found for samples T650_LP and T650_HP, the deposition rate increases from 8 to 21 nm/h, increasing by a factor of 2.6 times. As shown in Fig. 2, the sharp diffraction peak becomes much broader when MS pressure is increased from 0.006mbar in sample T700_LP to 0.06mbar in sample T700_HP. Both films contain nanocrystalline grains, but the grain size decreases significantly from around 100 nm for T700_LP to only 10 nm for T700_HP. Clearly, better crystallinity is achieved with the lower MS pressure. Comparing samples T650_LP and T650_HP, the broad diffraction peak in XRD

patterns observed in T650_LP disappears in T650_HP, which means the increase in pressure inhibits the nucleation of SiC nuclei, and causes the microstructure transition from nc-SiC to pure a-SiC. This again demonstrates that at a given temperature higher MS pressure induces more disorder to the microstructure to the deposited SiC film, and the transition from c-SiC to a-SiC can be achieved by varying MS pressure.

3.2 Hydrogen concentration and chemical order investigation

The hydrogen atomic concentrations were revealed by SIMS depth profiles analysis and measured results are shown in Fig. 4 for the samples prepared with MS pressure of 0.06mbar at different temperatures. The hydrogen atomic concentration in samples T700_HP, T650_HP and T600_HP is about 2.9×10^{21} cm^{-3}, 1.1×10^{22} cm^{-3} and 1.7×10^{22} cm^{-3}, respectively, which corresponds to compositional concentrations of 2.9 %, 11 % and 17 % (the precision of SIMS analysis for SiC material is around ±15 %). The hydrogen atomic concentration is quite uniform throughout the film thickness (as shown by SIMS depth profiles), decreases significantly at elevated temperatures.

Fig. 4. Hydrogen depth profiles by SIMS measurements.

The measured FTIR spectra are shown in Fig. 5. The centre position and full-width at half-maximum (FWHM) of the absorption band of Si–C bond are summarized in Table 2 for comparison. According to the TEM analyses, samples T700_HP, T700_LP and T650_LP are composed of nanocrystalline SiC in microstructure. The Si–C bond in the crystalline configuration corresponds to the sharp symmetrical absorption band with the peak position being very close to that of single-crystalline 3C-SiC (798 cm^{-1}) [30], although a small red shift and broadening of the peak are observed in those samples (as illustrated in Fig. 5 and Table 2), which could be due to defects and strained bonds at the grain boundaries or at the amorphous/crystal grain boundaries. The FWHM of Si–C absorption band increasing from 37

cm^{-1} for sample T700_LP to 81 cm^{-1} for sample T700_HP indicates that the chemical order of deposited SiC decreases with increasing MS pressure. While the FWHM of Si–C absorption band for samples T700_LP and T650_LP is very similar, though the grain size of sample T650_LP is much smaller than that of sample T700_LP. It indicates that better chemical order is achieved with lower MS pressure. Samples T650_HP and T600_HP, which are amorphous in physical structure as revealed by TEM and XRD, the FWHM of the Si–C absorption band is larger than 170 cm^{-1} (as shown in Fig. 5 and Table 2). Red shifts of the peak positions, from 794 to 757 cm^{-1}, and 746 cm^{-1}, respectively, were also observed for those two samples. This demonstrates degradation in the chemical order in those amorphous samples.

Fig. 5. FTIR spectra of SiC films deposited on Si substrates under various conditions.

Table 2. The center position and FWHM of Si–C absorption band obtained by FTIR spectrum measurements.

Given that SIMS measurements show hydrogen concentrations of more than 10% in a-SiC films, if the hydrogen atoms were forming Si–H_n bonds they should be easily detected by FTIR. The typical absorption band from the Si–H bond, Si–H_2 (dihydride) group, and $(Si–H_2)_n$ (polyhydride) group is located between 2000 and 2150 cm^{-1} [31]. The oscillator strength of Si-H bond stretching bands are enhanced by attaching C to Si [32], so the absence of absorption bands in this region, as shown in Fig. 5, indicates that Si–H_n (n = 1, 2, 3) bond density is below the detection limit of FTIR. Similarly, the lack of significant absorption bands in the range of 2800 to 3100 cm^{-1}, shown in Fig. 5, indicates that either the C–H_n (n = 1, 2, 3) bond density is very low in the film [27], or C–H_n (n = 1, 2, 3) bonds have very weak FTIR absorption strength. Quite a few papers have been published on hydrogen states, hydrogen concentration, and hydride bond density in a-SiC films [19, 27, 32-36], but possible disappearance of the absorption band of C–H_n (n = 1, 2, 3) bonds still remains as a

controversial issue. Nonetheless, the following factors lead us to believe that most of hydrogen exists as $C–H_n$ (n = 1, 2, 3) bonds in samples T650_HP and T600_HP: (1) the absorption band of the Si-C bond and $Si–(CH3)_n$ (n = 1, 2, 3) bonds sometimes overlap each other [32], (2) the oscillator strength of C–H bonds can be significantly reduced by the bonding environment [32], and (3) the significant reduction of hydrogen concentration (as revealed by SIMS) and the improvement of chemical order (shown by Si–C peak position and FWHM in FTIR spectra) at elevated temperatures. This means that the weak oscillator strength of C–H bond makes its absorption band in FTIR spectra unnoticeable.

4. Conclusions

Deposition of crystalline and amorphous SiC films on Si(100) substrates was demonstrated using MS as a single precursor by a conventional low-pressure chemical vapor deposition method in a hot-wall reactor, the temperature range was 600-700 ºC and no dilution gas was employed. Structural transitions from a-SiC to c-SiC were observed by varying the deposition temperature and MS pressure. The grain size decreases with increasing MS pressure at a given temperature and also decreases with reducing temperature at a given MS pressure. The deposition rates are exponentially dependent on the substrate temperature with the activation energy of around 2.6 eV. The hydrogen concentration decreased with increasing deposition temperature, with only 2.9 % in the c-SiC deposited at 700 ºC but higher than 10% in the a-SiC films. No hydride bonds were found in the a-SiC films by FTIR measurements. The improvement of chemical order was found for SiC films deposited at elevated deposition temperature.

Acknowledgements

This work at Griffith University was supported by the Australian Research Council and the Australian Institute of Nuclear Science and Engineering. The authors would like to express

sincere thanks to Anya Yago for conducting the XRD measurements and to Ross Steven for his assistance with the FTIR spectroscopy measurements.

References

[1] S.Y. Myong and K.S. Lim, Appl. Phys. Lett. 86 (2005) 033506.

[2] S.Y. Myong, K.S. Lim and J.M. Pearce, Appl. Phys. Lett. 87 (2005) 193509.

[3] M.W.M. van Cleef, R.E.E. Schropp, and F.A. Rubinelli, Appl. Phys. Lett. 73 (1998) 2609.

[4] S.Y. Myong, H.K. Lee, E. Yoon, and K.S. Lim, J. Non-Cryst. Solids 298 (2002) 131.

[5] S. Miyajima, M. Sawamura, A. Yamada, M. Konagai, J. Non-Cryst Solids 354 (2008) 2350.

[6] I. Martín, M. Vetter, A. Orpella, J. Puigdollers, A. Cuevas, and R. Alcubilla, Appl. Phys. Lett. 79 (2001) 2199.

[7] Z. Chen, K. Prasada, C.Y. Li, P.W. Lu, S.S. Su, L.J. Tang, D. Gui, S. Balakumar, R. Shu, and R. Kumar, Appl. Phys. Lett. 84 (2004) 2442.

[8] Z. Gong, E.G. Wang, G.C. Xu and Y. Chen, Thin Solid Films 348 (1999) 114.

[9] K. Basa, Phys. Stat. Sol. (a) 195 (2003) 87.

[10] Z. Yu, I. Pereyra, M.M.P. Carreno, Sol. Energy Mater. Sol. Cells 66 (2001) 155.

[11] G. Soto, E.C. Samato, R. Machorro and L. Cota, J. Vac. Sci. Technol. A 16 (1998) 1311.

[12] Z. He, G. Carter, and J.S. Colligon, Thin Solid Films 283 (1996) 90.

[13] J.J. Cuomo, D.L. Pappas, J. Bruley, J.P. Doyle and K.L. Saenger, J. Appl. Phys. 70 (1991) 1706.

[14] D.R. Mckenzie, J. Phys. D 18 (1985) 1935.

[15] I. Pereyra, C.A. Villacorta, M.M.P. Carreno, R.J. Prado and M.C.A. Fantini, Brazilian J. Phys. 30 (2000) 533.

[16] M.N.P. Carreño, I. Pereyra, H.E.M. Peres, J. Non-Cryst. Solids 227 (1998) 483.

[17] A.R. Oliveira, and M.N.P. Carreño, Mater. Sci. Eng. B 128 (2006) 44.

[18] A. Kolodziej, Opto-Electron. Rev. 12 (2004) 21.

[19] Y.Suzaki, T. Shikama, S. Yoshioka, K. Yoshii, and K. Yasutake, Thin Solid Film 311 (1997) 207.

[20] I. Golecki, F. Reidinger, and J. Marti, Appl. Phys. Lett. 60 (1992) 1703.

[21] H. Nakazawa, and M. Suemitsu, J. Appl. Phys. 93 (2003) 5282.

[22] Y. Narita, A. Konno, H. Nakazawa, T. Itoh, K. Yasui, T. Endoh, and M. Suemitsu, Jap. J. Appl. Phys. 46 (2007) L40.

[23] C.W. Liu, and J.C. Sturm, J. Appl. Phys. 82 (1997) 4558.

[24] J. H. Boo, S.A. Ustin, and W. Ho, Thin Solid Films 343-344 (1999) 650.

[25] E.C. Sanchez and S.J. Sibener, J. Phys. Chem. B 106 (2002) 8019.

[26] J. Xu, W.J. Choyke, J.T. Yate Jr., Appl. Surf. Sci. 120 (1997) 279.

[27] M.S. Lee, and S.F. Bent, J. Phys. Chem. B 101 (1997) 9195.

[28] T. Kaneko, D. Nemoto, A. Horiguchi, and N. Miyakawa, J. Cryst. Growth 275 (2005) e1097.

[29] A.D. Johnson, J. Perrin, J.A. Mucha, and D.E. Ibbotson, J. Phys. Chem. 97 (1993) 12937.

[30] S. Kerdiles, A. Hairie, R. Rizk, and C. Guedj, Phys. Rev. B 63 (2001) 205206.

[31] M. Shinohara, T. Maehama, M. Niwano, Appl. Surf. Sci. 162-163 (2000) 161.

[32] H. Wieder, M. Cardona, and C.R. Guarnieri, Phys. Stat. Sol. (b) 92 (1979) 99.

[33] L. Calcagno, F. Giorgis, A. Markhtari, P. Musumeci and R. Reitano, Philos. Mag. B 80 (2000) 539.

[34] F. Finocchi and G. Galli, Phys. Rev. B 50 (1994) 7393.

[35] R. Saleh, L. Munisa, and W. Beyer, Sol. Energy Mater. Sol. Cells 90 (2006) 3449.

[36] S.S. Camargo Jr., M.N.P. Carreño, and I. Pereyra, J. Non-Cryst. Solids 338-340 (2004) 70.

Figure captions

Fig. 1. The dependences of the deposition rates on the substrate temperature and MS pressure.

Fig. 2. X-ray diffraction patterns for SiC films deposited under various conditions.

Fig. 3. (a) HRTEM image of sample T700_LP, (b) SAED patterns of sample T700_LP, the regular dot diffractions are from underlying Si substrate (c) HRTEM image of sample T700_HP, (d) SAED patterns of sample T700_HP, (e) HRTEM image of sample T650_HP, (f) SAED patterns of sample T650_HP, (g) HRTEM image of sample T600_HP, (h) SAED patterns of sample T600_HP, the regular dot diffractions are from underlying Si substrate.

Fig. 4. Hydrogen depth profiles by SIMS measurements.

Fig. 5. FTIR spectra of SiC films deposited on Si substrates under various conditions.

Table 1. Detailed growth conditions and SiC film thickness for different samples.

Sample label	Substrate	Deposition temperature (ºC)	Pressure of MS (mbar)	Thickness of SiC layer (nm)
T700_LP	Si	700	0.006	410
T700_HP	Si	700	0.06	1050
T650_LP	Si	650	0.006	82
T650_HP	Si	650	0.06	210
T600_LP	Si	600	0.006	11
T600_HP	Si	600	0.06	50

Table 2. The center position and FWHM of Si–C absorption band obtained by FTIR spectrum measurements.

Sample label	Centre position of the Si–C bond absorption band (cm^{-1})	FWHM of the Si–C absorption band(cm^{-1})
3C-SiC single crystal	798	5.7
T700_LP	796	37.1
T700_HP	792	80.6
T650_LP	790	38.7
T650_HP	757	177.4
T600_HP	746	193.5

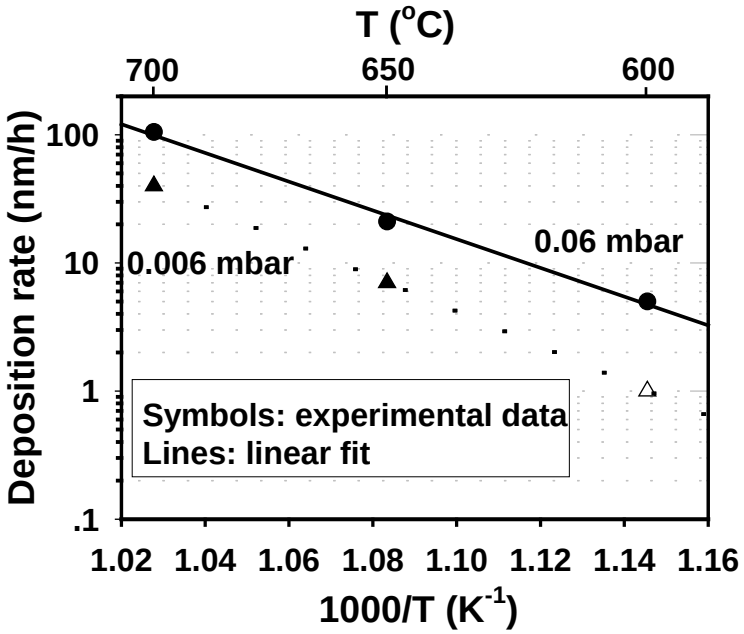

Fig. 1. The dependences of deposition rates on the substrate temperature and MS pressure.

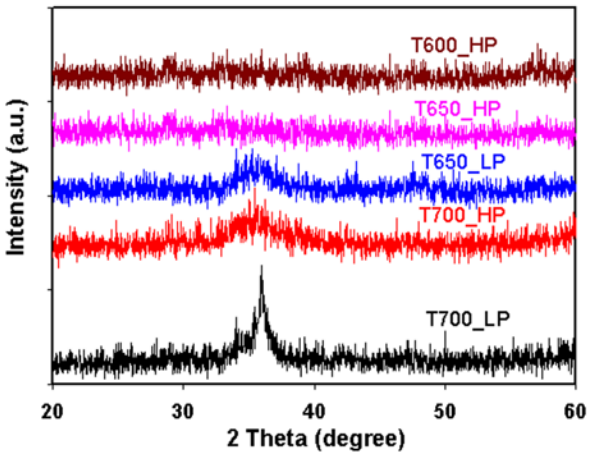

Fig. 2. X-ray diffraction patterns for SiC films deposited under various conditions.

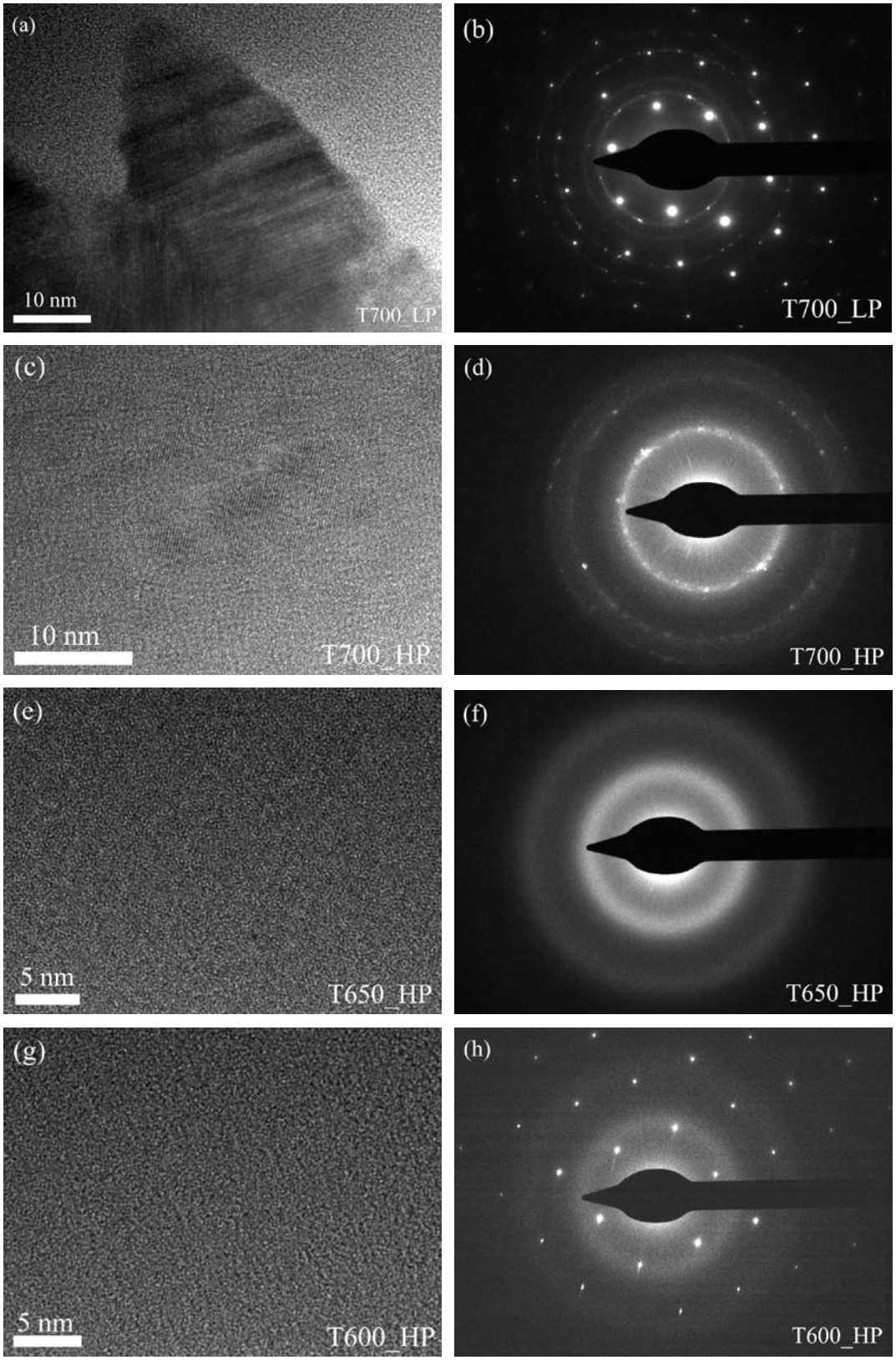

Fig. 3. (a) HRTEM image of sample T700_LP, (b) SAED patterns of sample T700_LP, the regular dot diffractions are from underlying Si substrate, (c) HRTEM image of sample

T700_HP, (d) SAED patterns of sample T700_HP, (e) HRTEM image of sample T650_HP, (f) SAED patterns of sample T650_HP, (g) HRTEM image of sample T600_HP, (h) SAED patterns of sample T600_HP, the regular dot diffractions are from underlying Si substrate.

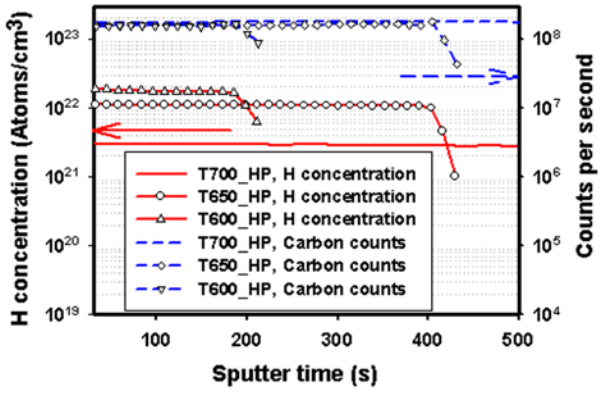

Fig. 4. Hydrogen depth profiles by SIMS measurements.

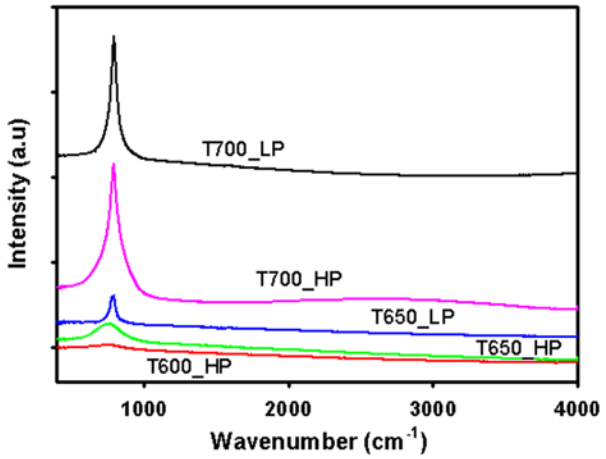

Fig. 5. FTIR spectra of SiC films deposited on Si substrates under various conditions.